SCIENTIFIC BULLETIN
OF
THE POLITEHNICA UNIVERSITY OF TIMISOARA

Vol. 63(77), Issue 2 MATHEMATICS–PHISYCS 2018

SOME PROPERTIES OF CORTICAL BONES

Ioana Ramona IOSIF

Abstract

In this paper are presented: structure of the bone tissue, anisotropic linear-elastic models of cortical bone and Analysis numerical propagation of a cracks into the cortical bone. To determine the fracture mechanics parameters at the crack tip, the finite element method was implemented in the FRANC2D / L 1.5 software. [1]

Keywords and phrases: *cortical bone, anisotropic, FRANC2D / L*

1 The structure of the bone tissue

The tissue has a complex hierarchical structure (Figure 1) which, due to its reduced density, results in a unique combination of properties: high strength and toughness, good stiffness, absorption capacity of deformation energy, Taylor (2010).

Also, this complex structure allows the bone tissue to perform important mechanical, biological and chemical functions, Sabet(2018):

• The structural support, ensuring body shape and weight support;

• It forms cavities for the protection of internal organs (the cranial box, thorax box, vertebral canal, etc.);

• Mineral ion homeostasis, bone tissue depositing 99% of the total $Ca2+$ in the body, 85% of the total phosphorus and 66% of the total magnesium);

• The spongy tissue of the epiphyses hosts the hematopoietic tissue (red marrow);

• The regenerative function that provides bone remodeling, healing of cracks and fractures. Bone tissue is divided into two broad categories, namely, compact bone tissue (osul cortical) and spongy bone (trabecular bone), see Figure 1. The compact bone tissue, accounting for 80% of the bone mass, represents a dense structure that contributes to strength and rigidity of the bone. It is located in the diaphysis of the long bones and in the cortical bones. Spongy bone tissue forms a less dense structure and is located in the central area of short bones, epiphyses of long bones

[1] MSC (2010): 74R99

and diploid bones. It is responsible for the absorption of deformation energy and the distribution of forces in the body. At the nanometric scale, collagen molecules and apatite crystals constitute collagen mineralized with a diameter of about 100 nm and a length of several μm, Sabet (2016), see Figure 1.

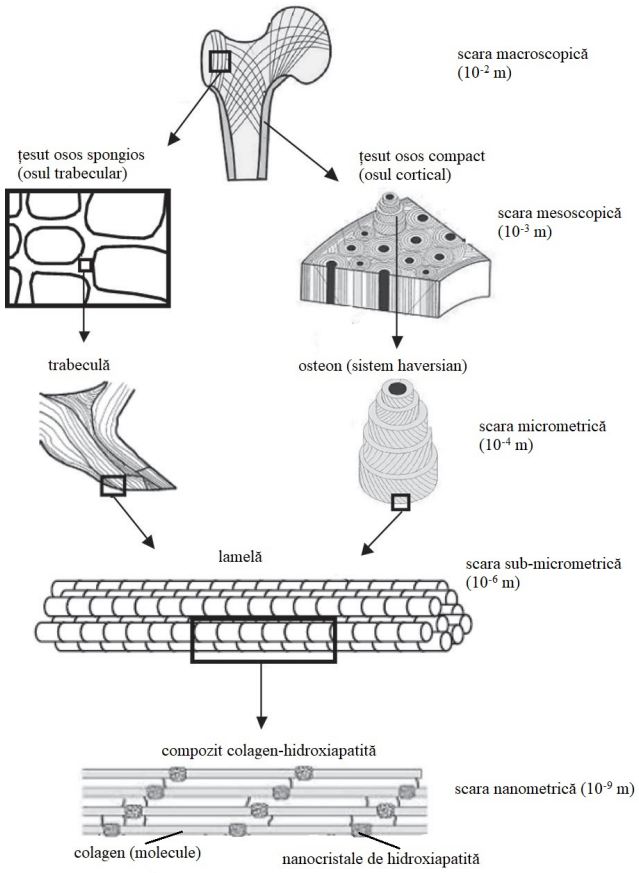

Figure 1:

These mineralized fibers, placed parallel to each other, form sub-micrometric scaffolds with a thickness of 3-7 μm, called lamellas. On a micrometric scale, the assembling of the lamellae leads to the formation of a number of tissues, the compact bone and the spongios. Compact (cortical) structure, approximately 4-20 lamels, not concentrically disposed around a vascular channel (haversian canal) forming the osteon, 200-300 μm in diameter a few mm. Between the osteons is the interstitial tissue, formed by remnants of the aged osteoarthritis, resulting from the bone remodeling process. Separation is provided by a cement line containing less collagen

(mesoscopic scale, see Figure 2).

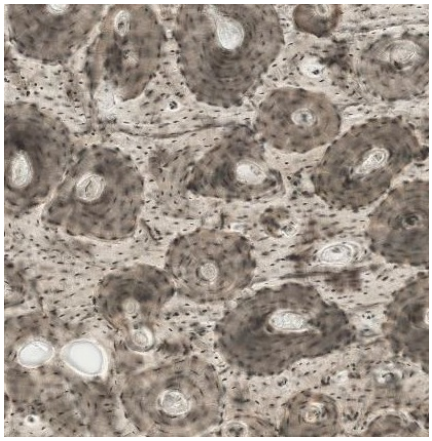

Figure 2:

In the structure of the spongy trabecular bone, the lamelele are assembled into branched trabecular forming a network that delimits areolele of different shapes and sizes. Areas contain connective tissue, blood vessels, nerve endings, and bone marrow. Thus, on a mesoscopic scale results a cellular structure illustrated in Figure 3. On a macroscopic scale the bone contains both compact tissue and spongy tissue.

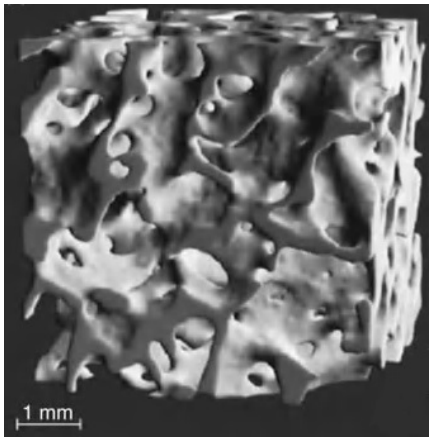

Figure 3:

The composition of the human bone depends on a large number of factors: sex, age, type of tissue, site of sampling, Katz (2008). Thus, bone tissue is thought

to contain $32-44\%$ organic substance (mainly collagen), $33-43\%$ minerals (as hydroxyapatite) and $15-25\%$ water, Sabet. (2016).

2 Anisotropic linear-elastic models of cortical bone

Although in reality bone-elastic tissue exhibits visco-elastic behavior, both in mechanical tests at low velocities and in the numerical analysis of stress and deformation state, it is considered, in an acceptable approximation, an anisotropic solid with a linear-elastic behavior, Katz (2008).

2.1 Tensions and deformations

The state of tension is known at a point P of a solid if the voltages that act on three orthogonal planes that pass through this point are known. In Figure 4, these are represented by even the coordinate planes of the orthogonal Cartesian system $x_1x_2x_3$.

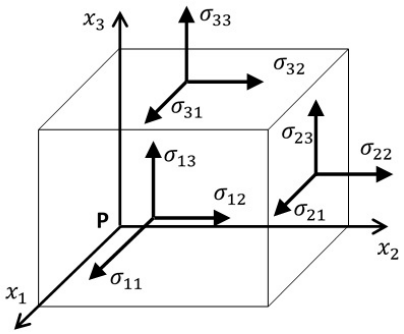

Figure 4: The state of tension at a point of a required solid

In other words, the voltage state at point P is defined by the voltage tensor with, a second-order tensor that can be represented by the array of:

$$\sigma = [\sigma] = \begin{bmatrix} \sigma_{11} & \sigma_{12} & \sigma_{13} \\ \sigma_{21} & \sigma_{22} & \sigma_{23} \\ \sigma_{31} & \sigma_{32} & \sigma_{33} \end{bmatrix} \tag{1}$$

where the tensions are normal tensions, and tensions are shear stresses (or tensile stresses). Tensions on the lines of this array act in the planes on which the coordinate

axes are normal. From the equilibrium conditions of the volume element illustrated in Figure 4 it is demonstrated that the voltage tensor is a symmetric tensor (i.e.):

$$\sigma = \begin{bmatrix} \sigma_{11} & \sigma_{12} & \sigma_{13} \\ \sigma_{21} & \sigma_{22} & \sigma_{23} \\ \sigma_{31} & \sigma_{32} & \sigma_{33} \end{bmatrix} = \begin{bmatrix} \sigma_1 & \sigma_6 & \sigma_5 \\ \sigma_6 & \sigma_2 & \sigma_4 \\ \sigma_5 & \sigma_4 & \sigma_3 \end{bmatrix} \tag{2}$$

In relation (2) the notation contraction is used, by the rule:

$$\alpha = i, \text{pentru} i = j; \alpha = 9 - i - j, \text{pentru} i \neq j \tag{3}$$

The contraction of the notation defined by the rule (3) makes it possible to represent the voltage tensor through the matrix of the column:

$$\{\sigma\} = \begin{Bmatrix} \sigma_1 \\ \sigma_2 \\ \sigma_3 \\ \sigma_4 \\ \sigma_5 \\ \sigma_6 \end{Bmatrix} \tag{4}$$

A certain point P of the solid required will move to P', the travel vector (a first-order tensor) being defined by the three components according to the coordinate axes:

$$u = u_i = (u_1, u_2, u_3), \quad i = 1, 2, 3 \tag{5}$$

In order to study the state of deformation of a solid-called Lagrange strain Ensor T is defined:

$$L_{ij} = \frac{1}{2} \left(u_{i,j} + u_{j,i} + u_{k,i} u_{k,j} \right) \tag{5}$$

where is the deformation gradient, Sadd (2014):

$$u_{i,j} = \frac{\partial u_i}{\partial x_j}$$

(6)

In the field of small deformations, ie, the second order term is neglected, and the deformation tensor it is:

$$\varepsilon = \varepsilon_{ij} = \frac{1}{2}\left(u_{i,j} + u_{j,i}\right)$$

(7)

Specific linear deformations (or specific lenghts for) expressing elongation per unit of length:

$$\varepsilon_{11} = \frac{\partial u_1}{\partial x_1} = \varepsilon_1;\ \varepsilon_{22} = \frac{\partial u_2}{\partial x_2} = \varepsilon_2;\ \varepsilon_{33} = \frac{\partial u_3}{\partial x_3} = \varepsilon_3$$

(8)

and specific angular deformations (or specific glides for) measures the change of right angles between two orthogonal directions:

$$2\varepsilon_{12} = 2\varepsilon_{21} = \left(\frac{\partial u_1}{\partial x_2} + \frac{\partial u_2}{\partial x_1}\right) = \varepsilon_6;$$

$$2\varepsilon_{23} = 2\varepsilon_{32} = \left(\frac{\partial u_2}{\partial x_3} + \frac{\partial u_3}{\partial x_2}\right)\varepsilon_4;$$

$$2\varepsilon_{31} = 2\varepsilon_{13} = \left(\frac{\partial u_3}{\partial x_1} + \frac{\partial u_1}{\partial x_3}\right) = \varepsilon_5.$$

(9)

In the relations (8) and (9) the same notation shrinkage was used. The deformation tensor is a symmetric tensor of the second order that can be represented in the matrix form:

$$\varepsilon = [\varepsilon]\begin{bmatrix} \varepsilon_{11} & \varepsilon_{12} & \epsilon_{13} \\ \varepsilon_{21} & \varepsilon_{22} & \varepsilon_{23} \\ \varepsilon_{31} & \varepsilon_{32} & \varepsilon_{33} \end{bmatrix} = \begin{bmatrix} \varepsilon_1 & \frac{\varepsilon_6}{2} & \frac{\varepsilon_5}{2} \\ \frac{\varepsilon_6}{2} & \varepsilon_2 & \frac{\varepsilon_4}{2} \\ \frac{\varepsilon_5}{2} & \frac{\varepsilon_4}{2} & \varepsilon_3 \end{bmatrix}$$

(10)

Geometric representation of deformations in the plane is illustrated in Figure 5, the approach being similar in the coordinate planes and x_2x_3 and x_3x_1.

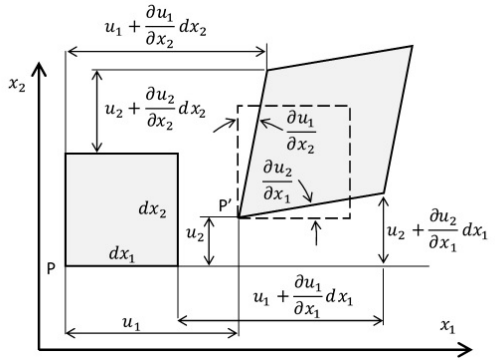

Figure 5: Deformation state

The connection between the voltage tensor and the deformation tensor is achieved with the aid of the elasticity tensor which contain our parameters of material:

$$\sigma = C_{\varepsilon} \tag{11}$$

or

$$\sigma_{ij} = C_{ijkl}\varepsilon_{kl} \tag{12}$$

Therefore,for a material with linear-elastic behavior, the writing of the constitutive equations (Hooke's law) is based on the hypothesis that each component of the voltage tensor is expressed by a linear combination of all the components of the deformation tensor. Tensor elasticity is a tensor of order 4 which contains, in general, 81 components ( ). Because voltage and strain tensors are symmetrical tensors:

$$\sigma_{ij} = \sigma_{ji},\ \varepsilon_{ij} = \varepsilon ji, \tag{13}$$

tensor elasticity meets conditions, Barbero (2008) and Saddam (2014):

$$C_{ijkl} = C_{jikl} = C_{ijlk} = C_{jilk} \tag{14}$$

Thus, the number of independent components decreases from 81 to 36, and the elasticity tensor can be represented by a matrix, the constitutive equations (12) becoming in the matrix form, by the contraction of the notation:

$$\begin{Bmatrix} \sigma_1 \\ \sigma_2 \\ \sigma_3 \\ \sigma_4 \\ \sigma_5 \\ \sigma_6 \end{Bmatrix} = \begin{bmatrix} C_{11} & C_{12} & C_{13} & C_{14} & C_{15} & C_{16} \\ C_{21} & C_{22} & C_{23} & C_{24} & C_{25} & C_{26} \\ C_{31} & C_{32} & C_{33} & C_{34} & C_{35} & C_{36} \\ C_{41} & C_{42} & C_{43} & C_{44} & C_{45} & C_{46} \\ C_{51} & C_{52} & C_{53} & C_{54} & C_{55} & C_{56} \\ C_{61} & C_{62} & C_{63} & C_{64} & C_{65} & C_{66} \end{bmatrix} \begin{Bmatrix} \varepsilon_1 \\ \varepsilon_2 \\ \varepsilon_3 \\ \varepsilon_4 \\ \varepsilon_5 \\ \varepsilon_6 \end{Bmatrix} \tag{15}$$

where are coefficients of elasticity, Boresi et al. (1993). Explaining the components of the stress tensor by the specific deformation energy derivatives according to the components of the deformation tensor, it is demonstrated that the number of independent elastic coefficients is reduced from 36 to 21 for a linear-elastic anisotropic material, Boresi et al. (1993). Thus, the constitutive equations (15), in the matrix form, become:

$$\begin{Bmatrix} \sigma_1 \\ \sigma_2 \\ \sigma_3 \\ \sigma_4 \\ \sigma_5 \\ \sigma_6 \end{Bmatrix} = \begin{bmatrix} C_{11} & C_{12} & C_{13} & C_{14} & C_{15} & C_{16} \\ C_{21} & C_{22} & C_{23} & C_{24} & C_{25} & C_{26} \\ C_{31} & C_{32} & C_{33} & C_{34} & C_{35} & C_{36} \\ C_{41} & C_{42} & C_{43} & C_{44} & C_{45} & C_{46} \\ C_{51} & C_{52} & C_{53} & C_{54} & C_{55} & C_{56} \\ C_{61} & C_{62} & C_{63} & C_{64} & C_{65} & C_{66} \end{bmatrix} \begin{Bmatrix} \varepsilon_1 \\ \varepsilon_2 \\ \varepsilon_3 \\ \varepsilon_4 \\ \varepsilon_5 \\ \varepsilon_6 \end{Bmatrix} \tag{16}$$

resulting in the elasticity matrix is symmetrical. Hooke's law (16) is often expressed using the matrix of compliance, which is the reverse matrix of elasticity, Barbero (2008):

$$\begin{Bmatrix} \varepsilon_1 \\ \varepsilon_2 \\ \varepsilon_3 \\ \varepsilon_4 \\ \varepsilon_5 \\ \varepsilon_6 \end{Bmatrix} = \begin{bmatrix} S_{11} & C_{12} & S_{13} & C_{14} & S_{15} & C_{16} \\ S_{21} & C_{22} & S_{23} & C_{24} & S_{25} & C_{26} \\ S_{31} & C_{32} & S_{33} & C_{34} & S_{35} & C_{36} \\ S_{41} & C_{42} & S_{43} & C_{44} & S_{45} & C_{46} \\ S_{51} & C_{52} & S_{53} & C_{54} & S_{55} & C_{56} \\ S_{61} & C_{62} & S_{63} & C_{64} & S_{65} & C_{66} \end{bmatrix} \begin{Bmatrix} \sigma_1 \\ \sigma_2 \\ \sigma_3 \\ \sigma_4 \\ \sigma_5 \\ \sigma_6 \end{Bmatrix} \tag{17}$$

3 The linear elastic orthotropic and that of cortical bone

A material with three mutually orthogonal planes of symmetry and that are called orthotropic. The most well-known examples are wood with cylindrical orthotropy and unidirectional fiber composites with a Cartesian ortho- pie, Barbero (2008). The model of the ortotropic material was used by Van Buskirk and Ashman (1981) to characterize the anisotropy of the cortical tissue. Their suggestion is based on experimental observations that the elastic properties of the tibia and human femur are different in the radial and circumferential directions of the transversal section (normal on the longitudinal axis of the bone). Conveniently, in Fig. 6 the coordinate planes are even the symmetry planes of the material.

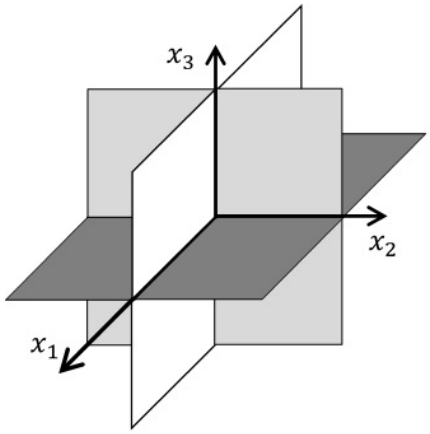

Figure 6: The planes of symmetry for an orthotropic material acid, Sadd (2014)

From the condition of symmetry to plan it follows that the following coefficients of elasticity are canceled, Barbero (2008) and Sadd (2014):

$$C_{i4} = C_{i5} = C_{46} = C_{56} = 0 \quad (i = 1, 2, 3) \tag{18}$$

Symmetry towards the plan leads to the following condition:

$$C_{16} = C_{26} = C_{36} = C_{45} = 0 \tag{19}$$

and the symmetry towards the plan is the result of the other two, without making any further changes to the elastic matrix.

Therefore, in the case of an orthoprophoric matrix the elasticity matrix will have 9 independent coefficients that characterize the behavior of such material. The constituent equations (16) and (17) in the matrix form are simplified as follows:

$$\begin{Bmatrix} \sigma_1 \\ \sigma_2 \\ \sigma_3 \\ \sigma_4 \\ \sigma_5 \\ \sigma_6 \end{Bmatrix} = \begin{bmatrix} C_{11} & C_{12} & C_{13} & 0 & 0 & 0 \\ C_{21} & C_{22} & C_{23} & 0 & 0 & 0 \\ C_{31} & C_{32} & C_{33} & 0 & 0 & 0 \\ 0 & 0 & 0 & C_{44} & 0 & 0 \\ 0 & 0 & 0 & 0 & C_{55} & 0 \\ 0 & 0 & 0 & 0 & 0 & C_{66} \end{bmatrix} \begin{Bmatrix} \varepsilon_1 \\ \varepsilon_2 \\ \varepsilon_3 \\ \varepsilon_4 \\ \varepsilon_5 \\ \varepsilon_6 \end{Bmatrix} \tag{20}$$

respectively

$$\begin{Bmatrix} \sigma_1 \\ \sigma_2 \\ \sigma_3 \\ \sigma_4 \\ \sigma_5 \\ \sigma_6 \end{Bmatrix} = \begin{bmatrix} S_{11} & S_{12} & S_{13} & 0 & 0 & 0 \\ S_{21} & S_{22} & S_{23} & 0 & 0 & 0 \\ S_{31} & S_{32} & S_{33} & 0 & 0 & 0 \\ 0 & 0 & 0 & S_{44} & 0 & 0 \\ 0 & 0 & 0 & 0 & S_{55} & 0 \\ 0 & 0 & 0 & 0 & 0 & S_{66} \end{bmatrix} \begin{Bmatrix} \varepsilon_1 \\ \varepsilon_2 \\ \varepsilon_3 \\ \varepsilon_4 \\ \varepsilon_5 \\ \varepsilon_6 \end{Bmatrix} \tag{21}$$

Matrix of Compliance was first deployed using the elastic properties of the experimentally determined material, as follows:

$$[S] = \begin{bmatrix} \frac{1}{E_1} & -\frac{\nu_{21}}{E_2} & -\frac{\nu_{31}}{E_3} & 0 & 0 & 0 \\ -\frac{\nu_{12}}{E_1} & \frac{1}{E_2} & -\frac{\nu_{32}}{E_3} & 0 & 0 & 0 \\ -\frac{\nu_{13}}{E_1} & -\frac{\nu_{23}}{E_2} & \frac{1}{E_2} & 0 & 0 & 0 \\ 0 & 0 & 0 & \frac{1}{G_{23}} & 0 & 0 \\ 0 & 0 & 0 & 0 & \frac{1}{G_{13}} & 0 \\ 0 & 0 & 0 & 0 & 0 & \frac{1}{G_{12}} \end{bmatrix} \tag{22}$$

In (22) represents the longitudinal modulus of elasticity in the direction the symmetry of the material, is the coefficient of transverse contraction (Poisson's coefficient) defined as the ratio of specific lenghts when applying normal tension , and is the transverse elastic modulus in the plane. An ortotropic material is characterized by a set of 9 independent elastic constants, out of a total of 12, due to the symmetry of the tensor, ie we have the following relationships fulfilled:

$$\frac{\nu_{12}}{E_1} = \frac{\nu_{21}}{E_2}, \ \frac{\nu_{13}}{E_1} = \frac{\nu_{31}}{E_3}, \ \frac{\nu_{23}}{E_2} = \frac{\nu_{32}}{E_3}$$

(23)

Also, the coefficients of the elastic matrix can be expressed by the elastic constants of the material, taking into account the relationship. Thus, Christmas, etc. (2018):

$$C_{11} = \frac{1-\nu_{23}\nu_{32}}{E_2E_3\Delta},\ C_{12} = \frac{\nu_{21}+\nu_{31}\nu_{23}}{E_2E_3\Delta} = \frac{\nu_{12}+\nu_{32}\nu_{13}}{E_1E_3\Delta}$$

$$C_{13} = \frac{\nu_{31}+\nu_{21}\nu_{32}}{E_2E_3\Delta} = \frac{\nu_{13}+\nu_{12}\nu_{23}}{E_1E_2\Delta},\ C_{22} = \frac{1-\nu_{13}\nu_{31}}{E_1E_3\Delta}$$

$$C_{23} = \frac{\nu_{32}+\nu_{12}\nu_{31}}{E_1E_3\Delta} = \frac{\nu_{23}+\nu_{21}\nu_{13}}{E_1E_2\Delta},\ C_{33} = \frac{1-\nu_{12}\nu_{21}}{E_1E_2\Delta}$$

$$C_{44} = G_{23},\ C_{55} = G_{13},\ C_{66} = G_{12}$$

(24)

where

$$\Delta = \frac{1-\nu_{12}\nu_{21}-\nu_{23}\nu_{32}-\nu_{31}\nu_{13}-\nu_{21}\nu_{32}\nu_{13}-\nu_{12}\nu_{23}\nu_{31}}{E_1E_2E_3}$$

(25)

Relationships (23) and (25) represent restrictions that experimentally determined elastic properties have to meet. Also, from (24) and (23) the restriction follows:

$$1-\nu_{ij}\nu_{ji} > 0,\ 0 < \nu_{ij} < \sqrt{\frac{E_i}{E_j}}\ (i,j=1,2,3;\ i \neq j)$$

(26)

4 The isotropic cross-sectional arthroplasty of the cortical bone

The transverse-isotropic material has an axis of symmetry, and consequently the planes containing this axis are symmetry planes (see Figure 7, the symmetry axis is). The transversal-isotropic model was used by Lang (1969), Katz and Ukraincik (1971) and Yoon and Katz (1976) to characterize cortical bone anisotropy.

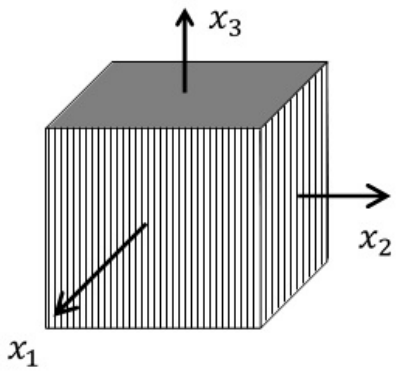

Figure 7: Symmetry axis for a transverse-isotropic material, Sadd (2014)

A transversal-isotropic material is characterized by a set of 5 independent elastic constants with the elastic matrix:

$$\begin{bmatrix} C_{11} & C_{12} & C_{13} & 0 & 0 & 0 \\ C_{12} & C_{11} & C_{13} & 0 & 0 & 0 \\ C_{13} & C_{13} & C_{33} & 0 & 0 & 0 \\ 0 & 0 & 0 & C_{44} & 0 & 0 \\ 0 & 0 & 0 & 0 & C_{44} & 0 \\ 0 & 0 & 0 & 0 & 0 & \frac{C_{11}-C_{12}}{2} \end{bmatrix} \tag{27}$$

and relationships between elastic properties, Katz (2008):

$$E_1 = E_2,\ \nu_{12} = \nu_{21},\ G_{12} = \frac{E_1}{2(1+\nu_{12})}$$

$$\nu_{31} = \nu_{32} = \nu_{13} = \nu_{23},\ G_{23} = G_{31} \tag{28}$$

5 Analysis numerical propagation of a cracks into the cortical bone (how mixed I-II)

The method of the finite element (MEF) is used into the biomechanics for The study TAD's behavior Mechanical Tissue bone, and examples are numerous: analysis st country voltage of femur human, Basuşa (1985); prediction breaking bone fem,

ral, Marco et al . (2018); estimate property mechanical of the vertebral bone, Brown et al. (2014); micrometric scale modeling of cortical bone breakage, Idkaidek and Jasiuk (2016), Li et al. (2013).

The conditions for starting the break cortical bone, for call into the module mixed I-II, is studied numeral into the continuation on The bending specimens NTI symmetric into the four points (AFPB - Asymmetric Four Point Bendspecimen)

5.1 Geometry of the AFPB specimen

The AFPB test was used in the mixed I-II breakdown study for ceramic materials, Suresh et al. (1990), granite, Razavi et al. (2017), alumina-PMMA, Marsavina, and others. (2013) or cortical bone, Zimmermann et al. (2009).

Geometry of the AFPB specimen and how to apply for the pattern used in this study are presented into the Figure 8, with thickness.

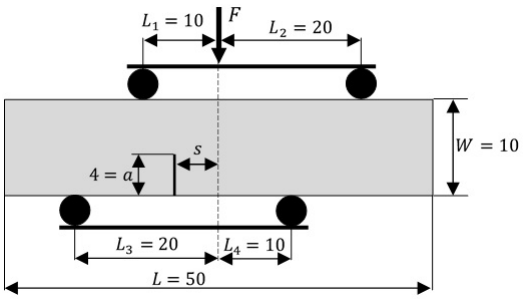

Figure 8: The AFPB test

Force is applied at a distance to the crack length (see Figure 8). Thus, the request into this plan (rift) is bending with force cutting efforts calculating with the relationships:

$$T = F\frac{L_2 - L_1}{L},\ M(s) = Ts \tag{29}$$

Into the case, the crack is produced only shear pure, obtaining a request in Mode II. Changing distance of the direction of force action and the crack plane, that is, for, is achieved applications into the module. C mixed ombi nation from Modules I and II are characterized through parameter to dimensional:

$$M^e = \frac{2}{\pi}\arctan\left(\frac{k_1}{k_{11}}\right)$$

(30)

The relationship (30), and the voltage for mode are the factors of intensity I of the request, so mode II, expressions of the form, Suresh et al. (1990)

$$K_1 = \varsigma\sqrt{\pi a}Y_1(a/W) = \frac{6M}{W^2 t}\sqrt{\pi a}Y_1(a/W) = 6\tau\frac{s}{W}\sqrt{\pi a}Y_1(a/W)$$

$$K_{ll} = \tau\sqrt{\pi a}Y_1(a/W)$$

(31)

Some functions depend on the report. Into the configuration, we have obtained superior values to about the results published by Suresh and others. (1990). Tensions and are produced by the bending and shearing requirements in the crack plane.

Mode I application ( ) is not obtained in antisymmetric configuration your presence into the Figure 8 because for any parameter value. Throughout, in the skeleton, a symmetric configuration is involved and i, for the epoch in the study.

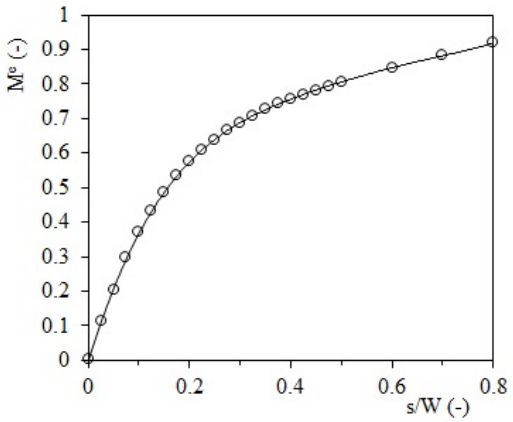

Figure 9: The variation of the M parameter is based on the position of the crack plane

Figure 9 is presented combination from Module I and Module II, in depending on the report, for:

5.2 Numerical Determination of Breaking Mechanics Parameters

To determine the fracture mechanics parameters at the crack tip, the finite element method was implemented in the FRANC2D / L 1.5 software developed at Cornell University, Wawrzynek (1991). Two types of isotropic and transverse isotropic

materials were studied comparatively. The working steps are further described for the AFPB sample shown in Figure 8.

The geometric modeling and meshing is performed with the CASCA pre-processor. The specimen geometry is made up of three sub-regions, especially because onvenabil for meshing (*G* e ometry menu commands Get Line LinesConnected). To control meshing parameters, such as number of elements and spacing along one side, the No. of segments and Ratio commands in the Subdivide menu are used (see Figure 10).

Figure 10: Determining the number of elements and spacing along the sides

Mesh Mesh specimen is carried out by selecting the menu items Q8 and technical quadratic bilinear 4side type recommended for the rectangular regions of the same apple nodes not on opposite sides (Figure 11).

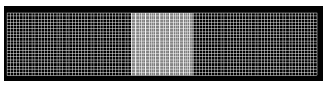

Figure 11: Specimen design

After completion meshed country save a CASCA file (e.g. afpb.csc, Write command) that can change then. Also, further analysis is saved a FRANC2D / L file, for example afpb.inp (Write Mesh command), file which import computing model.

The calculation of the number of mechanical parameters break with the method element Efe ctuează program is finished FRANC 2D / L.

Stage Understanding-processing assume the establishment conditions in which it is settled application: the type of problem, and material properties the limiting conditions.

Thickness taking account the specimen, equal with it was considered a matter of state plane stress (Pre-Process menu, submenu Problem Type, Plane Stress command).

Defined two material is first a behavior isotropic, and the second with a transversely isotropic behavior, properties, and Burstein Reilly (1975) considering specimen taken into the over axis The main material (Pre-Process menu, submenu Material / New Mat, ElastIso command / ElastOrth), through cancellation travel appropriate (Pre-Process menu, submenu fixity, Ind Fix command), and the load applied

applied applying the specimen (Pre-Process menu, submenu Loads, Load command Point).

Into the Processing steps and post processing is carried out analyze the stress and strain (Analysis menu, submenu Linear, Stiff direct command) and the viewing Results (Post-Process menu, submenu Contour command Stress / Strain). The program performs the linear-elastic analysis of the stress state using the direct elimination method (Gauss Removal Method).

Analyze parameters of mechanics breaking for the AFPB sample is being initiated through introduction of a edge cracks, whose sides are unencumbered (Modify menu, submenu New Crack, Non-Cohesive and EdgeCrack commands). Specify the edge node leading to the crack, the crack tip and the minimum number of finite elements on the crack length. At the tip of the crack, the program introduces a rosette consisting of 8 singular finite elements for modeling singularity, Figure 12.

For that a new one has emerged s STRUCTURE (specimen cracked), is carried out nine analysis of the state of tension and is calculated mechanical parameters Breaking: the angle the crack extension and the stress intensity factors and i. The FRANC2D / L program uses some techniques for calculation of stress intensity factors: extrapolation displacements, integral, the extension virtual crack. The method of extrapolation travel was used for evaluation stress intensity factors and in simulation of crack propagation on AFPB specimens (Post-Process menu, submenu fraction Mech, DSPCorr SIF / SIF History commands).

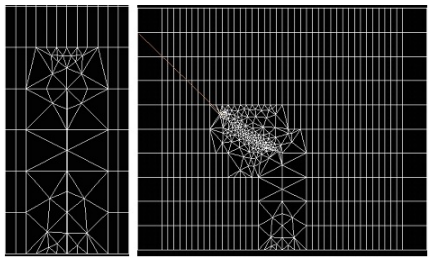

Figure 12: Starting the edge crack detail and propagating it in the II mode of application; isotropic material, increment 0.2 mm, 15 steps

Propagation crack is performed into the FRANC2D / L through standard technique or through technique automatic . Direction of propagation and the position new the peak of the crack is determined on the base of three initiation criteria into the module mixed, and namely: criterion blood circumfer Entiat maximum, criterion energy ie specific deformity minimum, respectively, the criterion ie force and maximum extension of the crack. After the establishment increment and a dir ECTI extension FIS hatred finite elements positioned along the path are removed and a

surface polygonal temporary intended for re-use mesh it is generated . Fissure initial It is exile nLet into the nine position of the tip and it is brought a rosette consisting of 8 triangular finite elements isobar a metric singular . Surface in the neighborhood ii crack it is discretized automatic. Into the Figure 12 is this t the outcome spread crack for an increment equal to and 15 consecutive steps using automatic technique (Modify menu, submenus Move Crack / Automatic, the Propagate command).

6 Results and conclusions

Trajectories crack, for the two materials, in Module I and Request Module II are presented into the Figures 13 and 14. Conditions critical crack extension, as the critical opening angle, are different for the two materials; same observation results and Figure 15, where for three stress situations (how I, how mixed I + II and module II) results number are represented into the compared to the solution criterion blood circumferential maximum (MTS criterion), Erdogan and Sih (1963). Validation results number and determination force critical crack extension assume Tests mechanical on cortical bone.

Also, it is proposed, in studiu a future use the XFEM method , implemented into the ABAQUS program, for modeling spread cracks into the case materials anisotrope.

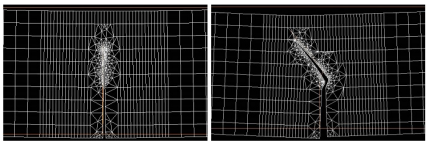

Figure 13: Fracture trajectory for load mode I (left - isotropic material, right - isotropic cross-sectional material

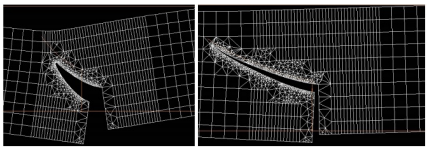

Figure 14: Fracture trajectory for load mode II (left - isotropic material, right - isotropic cross-sectional material

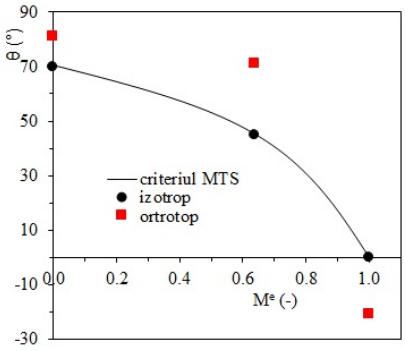

Figure 15: Critical angle of initiation to crack extension

References

[1] R. Baptista, A. Almeida, V. Infante (2016), Micro-crack propagation on a biomimetic bone-like composite material studied with the extended finite element method, Procedura Structural Integrity 1, 018-025.

[2] E.J. Barbero (2008), Finite Element Analysis of Composite Materials, CRC Press, Taylor and Francis Group.

[3] P .K. Basu, A. G. Beall, D. J. Simmons, M. W. Vannier (1985), 3-D femoral stress analysis using CT scans and p-version FEM, Biomaterials, Medical Devices, and Artificial Organs 13, 163-186.

[4] A. P. Boresi, R. J. Schmidt, O. M. Sidebottom (1993), Advanced Mechanics of Materials, 5th edition, John Wiley and Sons Ltd.

[5] K. R. Brown, S. Tarsuslugil, V. N. Wijayathunga, R. K. Wilcox (2014), Comparative finite element analysis: a single computational modeling method can estimate the mechanical properties of porcine and human vertebrae, Journal of the Royal Society Interface 11, 20140186.

[6] E. M. Christmas, A. Rabaea, M. F. Popa, C. I. Mihailov (2018), Crack propagation in the human bone. Mode I of Fracture, Annals of Science of "Ovidius" University Constanta 26, 59-70.

[7] F. Erdogan, G. C. Sih (1963), On the crack extension in plates by plane loading and transverses hear, Journal of Basic Engineering, Transactions of ASME 85, 519-525.

[8] A. Idkaidek, I. Jasiuk (2016), Cortical bone fracture analysis using XFEM-case study, International Journal for Numerical Methods in Biomedical Engineering, e02809.

[9] J. L. Katz, K. Ukraincik (1971), On the thean isotropic elastic properties of hydro xyapatite, Journal of Biomechanics 4, 221-227.

[10] J. L. Katz (2008), Mechanics of hard tissue, in: Peterson DR and Bronzino JD (ed.), Biomechanics. Principles and Applications, 9-20, CRC Press, Francis and Taylor Group.

[11] J .H. Kim, D. Kim, M. G. Lee (2013), Mechanics of cellular materials and its applications in: S. Li and D. Qian (ed.), Multi-scale Simulations and Mechanics of Biological Materials, 411-434, John Wiley and Sons Ltd.

[12] S. B. Lang (1969), Elastic coefficients of animal bone, Science 165, 287-288.

[13] S. Li, A. Abdel- Wahab, E. Demirci, V. V. Silberschmidt (2013), Fracture process in cortical bone: X-FEM analysis of micro-structured models, International Journal of Fracture 184, 43-55.

[14] M. Marco, E. Giner, R. Larrainzar-Garijo, J. R. Caeiro, M. H. Miguélez (2018), Modeling of femoral fracture using finite element procedures, Engineering Fracture Mechanics 196, 157-167.

[15] L. Marsavina, T. Sadowski, M. Knec (2013), Crack-propagation paths in four-pointbend Aluminum-PMMA, Engineering Fracture Mechanics 108, 139-151.

[16] S. M. J. Razavi, M. R. M. Aliha, F. Berto (2017), Applying a strain energy density criterion to obtain the mixed mode fracture load of granite rock tested with the cracked asymmetric four-point bend specimens, Theoretical and Applied Fracture Mechanics, In press, corrected proof, Available online 8 July 2017.

[17] D. T. Reilly, A. H. Burstein (1975), The elastic and ultimate properties of compact bone tissue, Journal of Biomechanics 8, 393-405.

[18] F. A. Sabet, A. R. Najafi, E. Hamed, I. Jasiuk (2016), Modeling of bone fracture and strength at different length scales: a review, Interface Focus 6, 20150055.

[19] M. H. Sadd (2014), Elasticity: Theory, Applications and Numerical 3 rd Edition, Elsevier.

[20] S. Suresh, C. F. Shih, A. Morrone, N. P. O'Dowd (1990), Mixed-mode fracture toughness of ceramic materials, Journal of the American Ceramic Society 73, 1257-1267.

[21] D. Taylor (2010), Why Do not Your Bones not made of Steel?, Materials Today 13, 6-7.

[22] W. C. Van Buskirk, R. B. Ashman R.B. (1981), The elastic moduli of bone, in: Cowin S.C. (ed.), Mechanical Properties of Bone AMD, vol 45, 131-143, American Society of Mechanical Engineers.

[23] P. A. Wawrzynek (1991), Discrete modeling of crack propagation: theoretical aspects and implementation issues in two and three dimensions, PhD Thesis, Cornell University, Ithaca.

[24] E. A. Zimmermann, M. E. Launey, H. D. Barth, R. O. Ritchie (2009), Mixed-mode fracture of human cortical bone, Biomaterials 30, 5877-5884.

[25] H. S. Yoon, J. L. Katz (1976), Ultrasonic wave propagation in human cortical bone: I. Theoretical considerations of hexagonal symmetry, Journal of Biomechanics 9, 407-412.

Ioana Ramona Iosif
Department of Mathematics,
Politehnica University of Timisoara,
P-ta Victoriei 2, 300006, Timisoara, ROMANIA
E-mail: ioana_ramo@yahoo.com